

Long-Term Stability Studies of a Semiconductor Photoelectrode in Three-Electrode Configuration

Srinivas Vanka^{1,2}, Kai Sun³, Guosong Zeng⁴, Tuan Anh Pham⁵, Francesca Maria Toma⁴, Tadashi Ogitsu⁵ and Zetian Mi^{1*}

¹ Department of Electrical Engineering and Computer Science, University of Michigan, Ann Arbor, 1301 Beal Avenue, Ann Arbor, MI 48109, USA

² Department of Electrical and Computer Engineering, McGill University, 3480 University Street, Montreal, Quebec, H3A 0E9, Canada

³ Department of Materials Science and Engineering, University of Michigan, 2300 Hayward Street, Ann Arbor, MI 48109, USA

⁴ Lawrence Berkeley National Laboratory, Chemical Sciences Division, 1 Cyclotron Road, Berkeley, CA 94720, USA

⁵ Lawrence Livermore National Laboratory, Quantum Simulations Group, 7000 East Avenue, L-413, Livermore, CA 94550, USA

* Corresponding author E-mail: ztmi@umich.edu; Phone: +1 734 764 3963

Experimental Section

MBE growth of n^+ -GaN nanowires on $n^+ \text{-} p$ Si. The nanowires are formed spontaneously under nitrogen-rich conditions without using any external metal catalyst, which lead to N-terminated surfaces, not only for their top c-plane but also for the surrounding nonpolar surfaces¹. The growth conditions included a substrate temperature ~ 730 °C, Ga beam equivalent pressure of 6×10^{-8} torr, Ge cell (*n*-type dopant) at 1050 °C, nitrogen flow rate of 1 standard cubic centimeter per minute, plasma forward power of 350 W, and growth duration of 2 h²⁻⁴.

Photoelectrode Preparation. The n^+ -GaN nanowires/ $n^+ \text{-} p$ Si photocathode was first diced into pieces of with areas between 0.1 and 0.25 cm² using a diamond pen. Ohmic contact to the photocathode was made by lightly smearing Ga-In eutectic paste on the backside of the sample, which was subsequently connected to a Cu-wire by using silver paste. The electrical connection was then encapsulated by using epoxy which was spread on a glass slide and covered the backside and edge of the sample to minimize any leakage current.

Photo-deposition of Pt co-catalyst nanoparticles. The prepared photoelectrode was mounted on a glass slide and placed in the bottom of a Pyrex chamber with a quartz window. Next, 10 µL of 0.2 M Chloroplatinic acid hydrate (99.9%, Sigma Aldrich) was used as Pt precursor, and 11 mL of CH₃OH (i.e., a hole scavenger) and 55 mL of Milli-Q water were poured into the Pyrex chamber. The chamber was subsequently evacuated using a vacuum pump for 10 min. Then the sample was irradiated using a 300 W xenon lamp (PerkinElmer, PE300BF) for 30 min for the photodeposition of Pt co-catalyst nanoparticles.

Regeneration of Pt Co-catalyst Nanoparticles. At the end of each cycle, the sample was mounted again on a glass slide for the photo-deposition of Pt co-catalyst nanoparticles. It is essential to avoid any unnecessary mechanical stress on the samples in this process. The glass slide was placed in Pyrex chamber, and 5-10 μ L of 0.2 M Chloroplatinic acid hydrate (99.9%, Sigma Aldrich), 11 mL of CH₃OH and 55 mL of Milli-Q water were added to the Pyrex chamber. The chamber was evacuated using a vacuum pump for 10 min. Then the sample was irradiated using a 300 W xenon lamp for 20-25 min. After the redeposition, the sample was dried with N₂ gun and ready for the next run.

Photoelectrochemical reaction. PEC experiments, including *J-V* characterization and stability measurements, were conducted in 0.5 M H₂SO₄ solution in a three-electrode configuration using Pt-decorated GaN/Si, silver chloride electrode (Ag/AgCl), and Pt wire as the working, reference, and counter electrode, respectively. A solar simulator (Newport Oriel) with an AM 1.5G filter was used as the light source, and the light intensity was calibrated to be 100 mW/cm² for all the experiments. Considering the long-term stability experiments, it is essential to regularly calibrate the intensity of solar simulator, which was done by using Newport-Power-818-ST-UV power meter. The conversion of the Ag/AgCl reference potential to a reversible hydrogen electrode (RHE) is calculated using Eqn. 1,

$$E_{(RHE)} = E_{Ag/AgCl} + E_{Ag/AgCl}^o + 0.059 \times pH \quad (1)$$

where $E_{Ag/AgCl}^o$ is 0.197 V, and pH of the electrolyte is nearly zero.

The ABPE of the photocathode was derived using Eqn. 2⁵,

$$ABPE (\%) = \left[\frac{|J_{ph} (mA.cm^{-2})| \times (V_{app} - V_{o,cathode})}{P_{tot} (mW.cm^{-2})} \right] \times 100 \quad (2)$$

where $V_{o,cathode} = 0 V$ vs RHE, J_{ph} is photocurrent density measured under applied bias (V_{app}) vs. RHE and P_{tot} is AM 1.5G one sun illumination (100 mW/cm²).

The Faraday efficiency ($\eta_{(Faraday)}$) for stability H₂ evolution measurements were calculated using Eqn. 3^{2, 5, 6}, which describes the ratio of average experimental (red dots) and theoretically calculated (black dots) H₂ production.

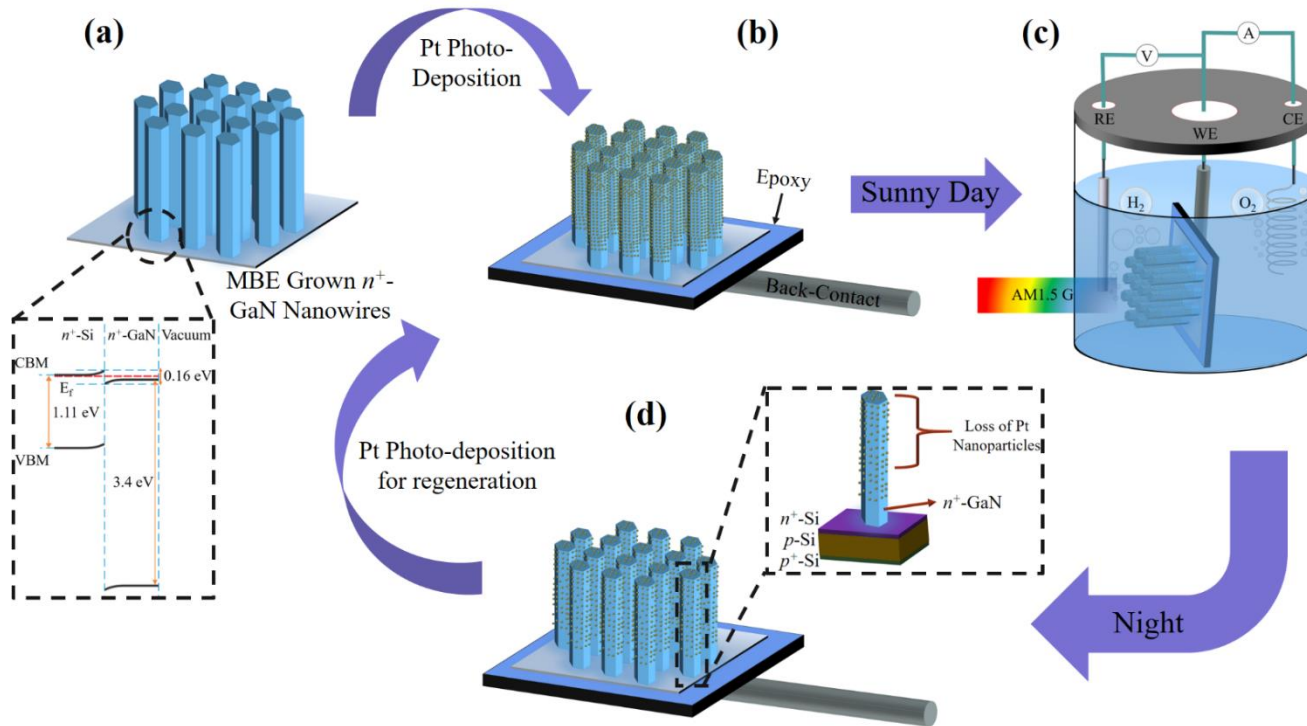
$$\eta_{(Faraday)}(\%) = \frac{2 \times n_{H_2}(t=T_0)[mol] \times F}{\int_0^{T_0} I [A] \cdot dt [s]} \times 100 \quad (3)$$

where I is the measured photocurrent, F is Faradaic constant (96485 C/mol) and n_{H_2} is the total amount of H₂ produced for a time duration T_0 . H₂ was detected by gas chromatograph (GC, Shimadzu GC-8A) equipped with a thermal conducting detector (TCD).

SEM and TEM Characterization. SEM images are taken using Hitachi SU8000 at an accelerating voltage of 10 kV. High angle annular dark field (HAADF)-STEM images were collected using a JEOL 2100F microscope with STEM aberration corrector operated at 200 kV. The TEM samples were prepared by scratching the nanowire surface with a tweezer/glass-slide and then mechanically transferring the GaN nanowires on the TEM copper grid.

AFM measurements. Nanometer scale lateral resolution scanning of a 1×1 μm² area before and after 10 h chronoamperometry testing were acquired by a commercial AFM system (Bruker Dimension ICON). A silicon tip with on nitride cantilever with nominal spring constant of 0.4 N/m was selected for this measurement. The surface mapping was obtained by Peak Force mode using low deflection setpoint and scan rate was set to 0.5 Hz to minimize the artifacts due to drifting, disturbance, etc.

ICP-MS measurements. ICP-MS measurements were conducted using a Perkin-Elmer Nexion 2000 ICP-MS machine. The electrolyte samples were collected at the end of a 24 h dark run, 1st, 46th, 96th, and 140th regeneration cycle. The calibrations were done using standard Ga and Pt (1000µg/mL) from Ultra Scientific with bismuth as internal standard.



Scheme S1. Pt catalyst regeneration process during stability experiment using (a) MBE grown n^+ -GaN nanowires on $n^+ - p$ Si photocathode. The band-diagram at the bottom shows the unique advantage of small conduction band offset between n^+ -GaN and n^+ -Si which allows efficient charge carrier extraction ². This photocathode first undergoes (b) Pt photo-deposition after electrode preparation, then followed by (c) the start of three-electrode stability experiment inside the glass chamber during a “sunny” day (AM 1.5G one-sun illumination). (d) After this run, the loss of Pt nanoparticles can be replenished, during “night” time, to Scheme 1(b) by doing Pt photo-deposition on the photocathode. Then the next cycle starts as shown in Scheme 1(c). This cycle consisting of stability run for 24 h, and subsequent Pt catalyst regeneration has been repeated more than 100 times throughout 3000 h.



Figure S1. STEM of Pt-decorated n^+ -GaN nanowires/ n^+ - p Si photocathode before the start of long-term stability experiments.

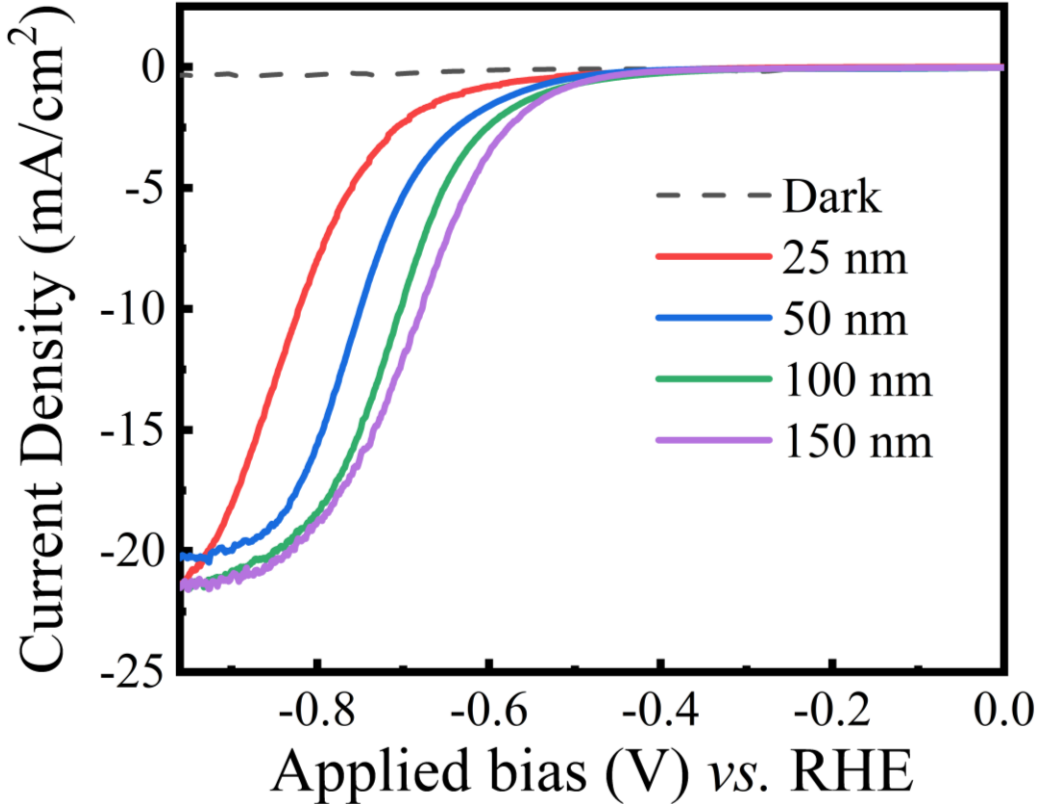


Figure S2. Comparison of J - V curves for planar n^+ -GaN protected n^+ - p Si (without Pt nanoparticles) with thicknesses: 25 nm (red color), 50 nm (blue color), 100 nm (green color) and 150 nm (pink color) under AM 1.5G one-sun illumination and dark (black color) conditions. The maximum saturation J for all the thicknesses at ~ -1 V vs. RHE is $\sim 20\text{-}22$ mA/cm^2 , which is consistent with the near-perfect conduction band-alignment between n^+ -GaN and Si (as shown in Figure 1(d)).

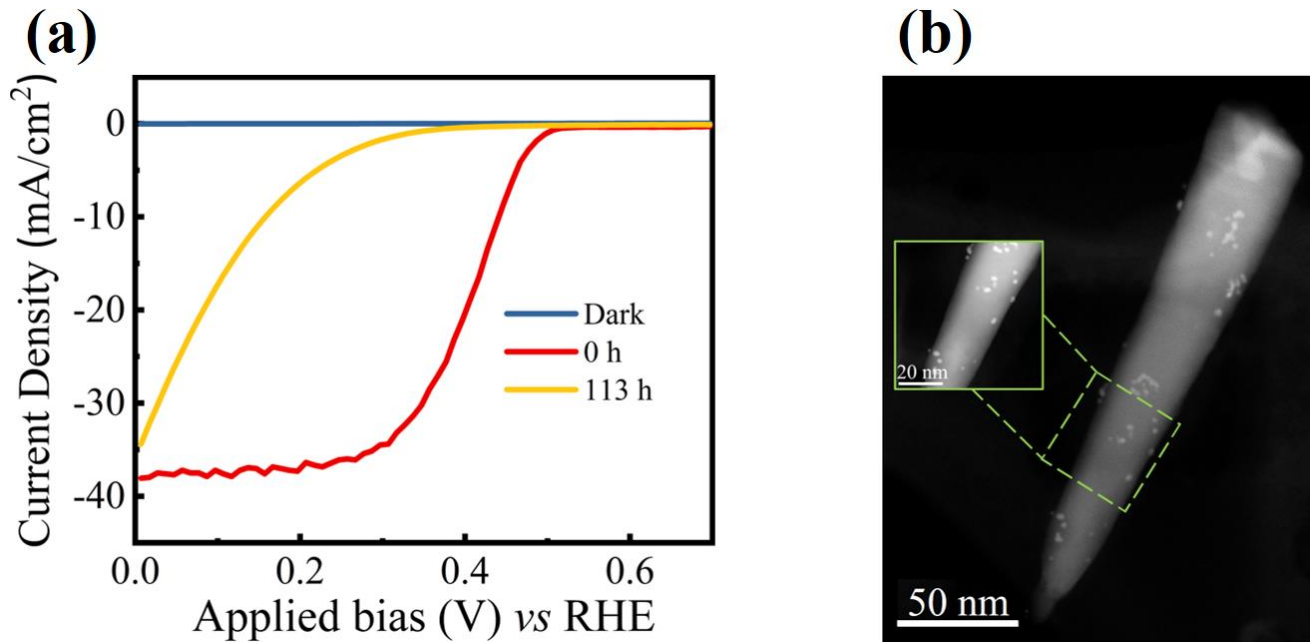


Figure S3. (a) J - V characteristics (from previous publication) of platinized n^+ -GaN nanowires/ n^+ - p Si photocathode in 0.5M H₂SO₄ under AM 1.5G one sun illumination for 0 h (red curve) and 113 h (orange curve) and dark condition (blue curve)². (b) STEM of Pt-decorated n^+ -GaN nanowires/ n^+ - p Si photocathode (from previous publication) after 50 h experiment². The Pt nanoparticles are reduced compared to Supp. Info. Figure 1 and the nanowire dimensions remained unchanged.

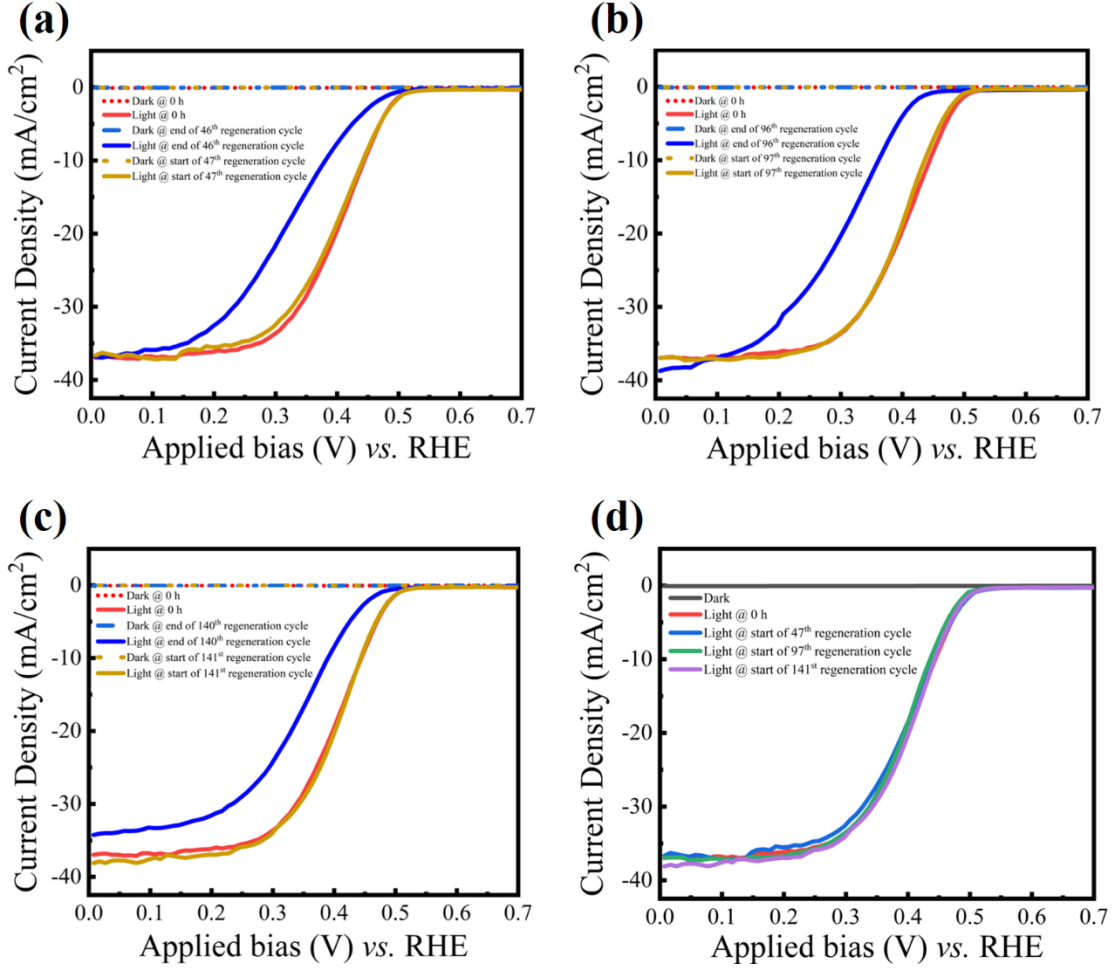


Figure S4. Comparison of LSV measured throughout the long-term stability testing under AM 1.5G one-sun illumination and dark. (a) LSV measured at the beginning of the long-term stabilizing testing (i.e., 0 h), at the end of the 46th cycle (i.e., 1003 h), and at the beginning of the 47th cycle (i.e., 1003 hr, after Pt-redeposition); (b) LSV measured at the beginning of the long-term stabilizing testing (i.e., 0 h), at the end of the 96th cycle (i.e., 2022 h), and at the beginning of the 97th cycle (i.e., 2022 hr, after Pt-redeposition) and (c) LSV measured at the beginning of the long-term stabilizing testing (i.e., 0 h), at the end of the 140th cycle (i.e., 3008 h), and at the beginning of the 141st cycle (i.e., 3008 hr, after Pt-redeposition). (d) LSV comparisons between 0 h (red), at the start of 47th cycle (blue), 97th cycle (green) and 141st cycle (pink) under AM 1.5G one-sun illumination in 0.5M H₂SO₄.

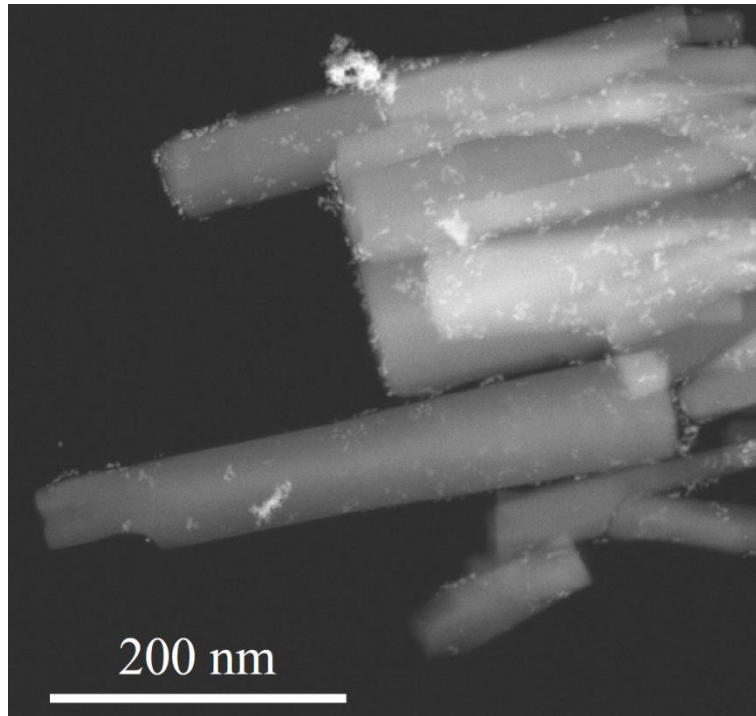


Figure S5. STEM image of Pt-decorated n^+ -GaN nanowires/ $n^+ \text{-} p$ Si photocathode at the end of the 140th regeneration cycle. It is seen that the Pt co-catalyst nanoparticles are reduced compared to Supp. Info. Figure 1. No noticeable etching of GaN nanowires was observed.

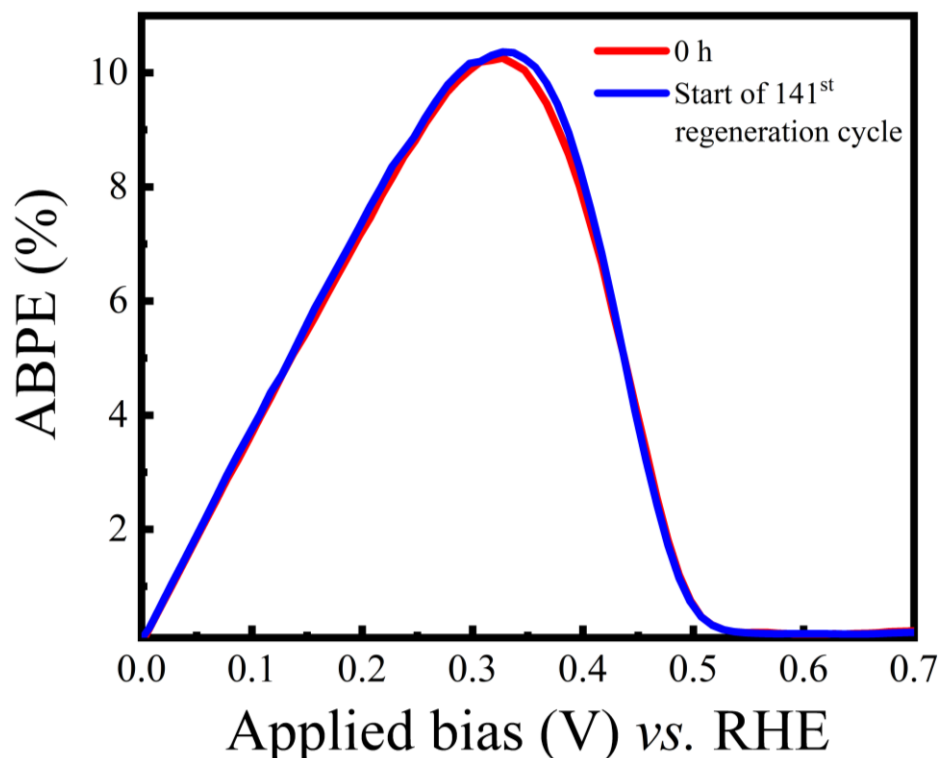


Figure S6. ABPE comparison between 0 h (red curve) and at the start of 141st regeneration cycle (blue curve). The ABPE for both the curves is ~10%.

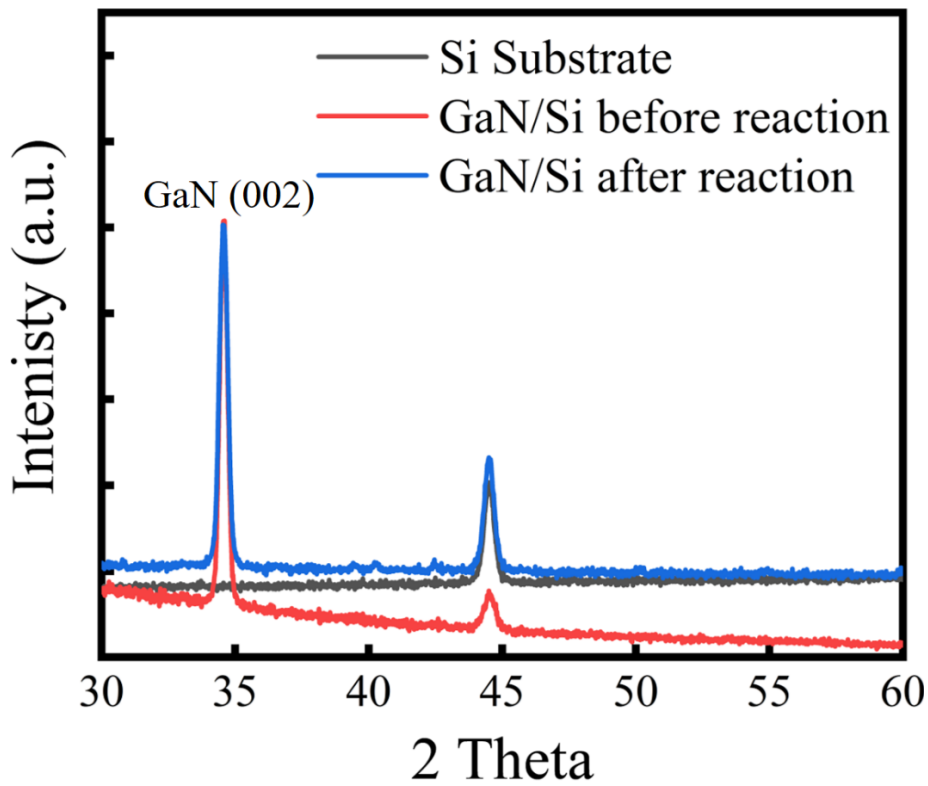


Figure S7. X-ray diffraction of GaN/Si photocathode before (red color) and after (blue color) PEC stability reaction. The wurtzite structure of the GaN nanowires was confirmed through the observation of the (002) peak in the XRD spectrum at $2\text{theta}=34.5^\circ$. The XRD spectrum for these samples is measured using a Rigaku SmartLab XRD.

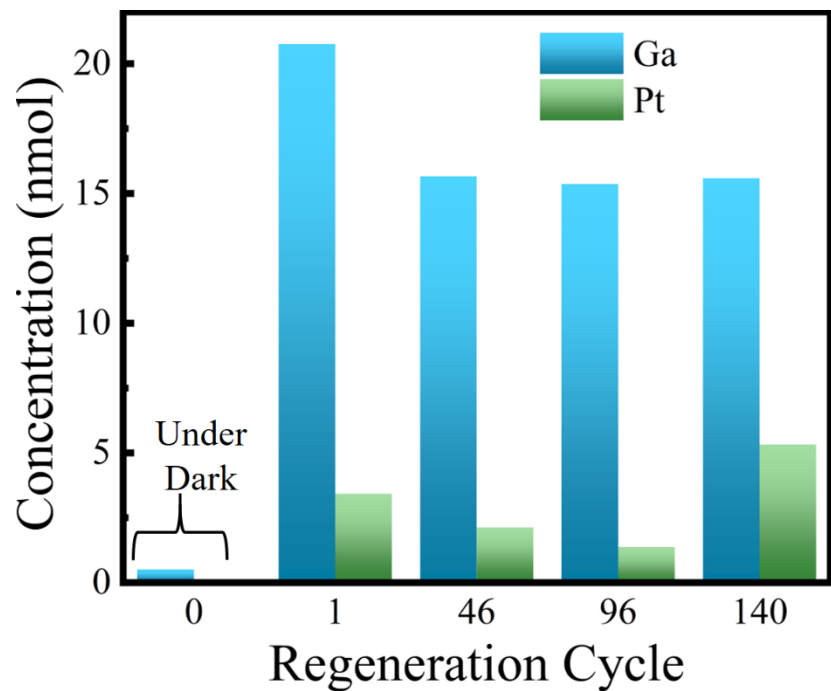


Figure S8. ICP-MS measurements of Ga and Pt elements (in nmol) at the end of 24 h dark experiment (shown as “0”), 1st, 46th, 96th and 140th regeneration cycle during the long-term stability of Pt/ n^+ -GaN nanowires/ n^+ -*p* Si.

Table S1. State-of-the-art stability, measured as J vs. t , of photocathodes and photoanodes for PEC in three-electrode configuration.

Materials	Electrolyte	J_{ph} (mA/cm ²) during stability test	ABPE (%)	Stability	pH	Ref
MoS ₂ /MoO/n ⁺ -p Si photocathode	0.5M H ₂ SO ₄	15	2 (approx.)	1440 h (at 0 V vs. RHE)	0	⁷
NiFe/Mo-doped BiVO ₄ /Ti/Sn photoanode	1M Borate buffer	2.7	3.6	1100 h (at 0.6 V vs. RHE)	7	⁸
NiCrO _x /TiO ₂ /np ⁺ - Si MW photoanode	1M KOH	4.6	1 (approx.)	2200 h (at ~1.6 V vs. RHE)	13.6	⁹
NiMo/NiSi/n ⁺ p Si MW photocathode	1M KOH	9.5	10.1	288 h (at 0.5 V vs. RHE)	14	¹⁰
Pt/TiO ₂ /Ti/n ⁺ -p Si photocathode	0.5M H ₂ SO ₄	17	8	300 h (at 0.3 V vs. RHE)	0	¹¹
α -Fe ₂ O ₃ photoanode	1M NaOH	0.95	1 (approx.)	1000 h (at 1.45 V vs. RHE)	14	¹²
Pt/TiO ₂ /Ti/n ⁺ -p Si photocathode	1M HClO ₄	22	NA	720 h (at 0.3 V vs. RHE); incident photon ($\lambda > 635$ nm)	0	¹³

Pt/TiO ₂ /Si MOS photocathode	1M HClO ₄	25	NA	1900 h (at 0.4 V <i>vs.</i> RHE); incident photon ($\lambda > 635$ nm)	0	¹⁴
NiO _x / <i>np</i> ⁺ Si photoanode	1M KOH	32	2.3	1200 h (at 1.73 V <i>vs.</i> RHE)	14	¹⁵
Pt/CdS/CuGa ₃ Se ₅ / (Ag,Cu)GaSe ₂	0.1M Buffer solution	8.79	NA	240 h (at 0 V <i>vs.</i> RHE)	7	¹⁶
Pt/ <i>n</i> ⁺ -GaN nanowires/ <i>n</i> ⁺ - <i>p</i> Si photocathode	0.5M H ₂ SO ₄	38	11.9	3000 h (at 0 V <i>vs.</i> RHE)	0	This work

Note: Mo/*np*⁺-Si photoanode showed long-term stability of ~ 4500 h (at 0 V *vs.* Pt)¹⁷. But the stability measurements were done under uncalibrated light source in HI solution, which is not water splitting.

Table S2. Summary of all regeneration cycles showing V_{on} , photocurrent density J_{ph} and dark current density J_d at the start and end of each cycle.

Regeneration Cycle	Start of cycle (h)	End of cycle (h)	V_{on} (V vs. RHE)		J_{ph} at 0 V vs. RHE (mA/cm ²)		J_d at 0 V vs. RHE (mA/cm ²)	
			Start	End	Start	End	Start	End
1	0	23	0.54	0.5	37	38	0.03	0.03
2	23	46	0.52	0.49	38	39	0.03	0.03
3	46	70	0.53	0.5	38	37	0.03	0.03
4	70	93	0.51	0.49	37	35	0.03	0.03
5	93	116	0.51	0.48	37	35	0.03	0.03
6	116	139	0.51	0.49	38	37	0.03	0.03
7	139	164	0.52	0.48	38	37	0.03	0.03
8	164	187	0.53	0.47	38	38	0.03	0.03
9	187	210	0.51	0.49	38	38	0.03	0.03
10	210	232	0.53	0.44	37	39	0.03	0.03
11	232	259	0.51	0.45	38	39	0.03	0.03
12	259	284	0.5	0.46	39	39	0.03	0.03
13	284	308	0.53	0.44	38	36	0.03	0.03
14	308	332	0.52	0.43	38	39	0.03	0.03
15	332	345	0.54	0.43	39	40	0.03	0.03
16	345	357	0.5	0.42	39	36	0.03	0.03

17	357	386	0.51	0.4	38	37	0.03	0.03
18	386	400	0.51	0.48	37	34	0.03	0.03
19	400	417	0.51	0.49	38	38	0.03	0.03
20	417	441	0.52	0.48	38	37	0.03	0.03
21	441	465	0.53	0.47	37	38	0.03	0.03
22	465	490	0.51	0.49	38	36	0.03	0.03
23	490	514	0.53	0.44	37	37	0.03	0.03
24	514	539	0.52	0.48	39	38	0.03	0.03
25	539	562	0.54	0.5	38	39	0.03	0.03
26	562	583	0.52	0.49	37	38	0.03	0.03
27	583	607	0.53	0.47	38	38	0.03	0.03
28	607	628	0.52	0.48	38	39	0.03	0.03
29	628	650	0.53	0.47	38	39	0.03	0.03
30	650	674	0.51	0.49	40	40	0.03	0.03
31	674	690	0.53	0.44	38	37	0.03	0.03
32	690	713	0.52	0.48	38	37	0.03	0.03
33	713	738	0.51	0.49	39	40	0.03	0.03
34	738	762	0.53	0.44	38	37	0.03	0.03
35	762	783	0.51	0.45	38	36	0.03	0.03
36	783	807	0.5	0.46	38	34	0.03	0.03
37	807	823	0.53	0.44	37	34	0.03	0.03
38	823	848	0.54	0.5	39	38	0.03	0.03
39	848	870	0.52	0.49	38	38	0.03	0.03

40	870	892	0.53	0.5	38	41	0.03	0.03
41	892	917	0.51	0.49	40	40	0.03	0.03
42	917	938	0.51	0.48	38	39	0.03	0.03
43	938	962	0.51	0.49	38	39	0.03	0.03
44	962	974	0.52	0.48	39	40	0.03	0.03
45	974	985	0.53	0.47	38	39	0.03	0.03
46	985	1003	0.51	0.49	38	40	0.03	0.03
47	1003	1024	0.53	0.44	39	38	0.03	0.03
48	1024	1046	0.51	0.45	38	39	0.03	0.03
49	1046	1075	0.5	0.46	37	38	0.03	0.03
50	1075	1095	0.54	0.43	38	38	0.03	0.03
51	1095	1115	0.51	0.48	38	39	0.03	0.03
52	1115	1139	0.51	0.49	38	37	0.03	0.03
53	1139	1159	0.52	0.48	38	33	0.03	0.03
54	1159	1172	0.53	0.47	38	34	0.03	0.03
55	1172	1197	0.51	0.49	37	42	0.03	0.03
56	1197	1222	0.53	0.44	38	40	0.03	0.03
57	1222	1242	0.51	0.45	39	38	0.03	0.03
58	1242	1263	0.5	0.46	38	33	0.03	0.03
59	1263	1277	0.53	0.44	37	39	0.03	0.03
60	1277	1285	0.51	0.45	38	37	0.03	0.03
61	1285	1308	0.54	0.48	38	40	0.03	0.03
62	1308	1326	0.52	0.48	40	38	0.03	0.03

63	1326	1353	0.53	0.47	38	37	0.03	0.03
64	1353	1379	0.54	0.5	38	39	0.03	0.03
65	1379	1399	0.52	0.49	38	41	0.03	0.03
66	1399	1423	0.53	0.5	38	39	0.03	0.03
67	1423	1440	0.51	0.49	37	41	0.03	0.03
68	1440	1464	0.51	0.48	38	33	0.03	0.03
69	1464	1480	0.51	0.49	38	35	0.03	0.03
70	1480	1504	0.52	0.48	38	33	0.03	0.03
71	1504	1514	0.53	0.47	38	40	0.03	0.03
72	1514	1531	0.51	0.49	38	38	0.03	0.03
73	1531	1556	0.53	0.44	37	32	0.03	0.03
74	1556	1580	0.51	0.45	38	38	0.03	0.03
75	1580	1604	0.53	0.44	38	39	0.03	0.03
76	1604	1629	0.51	0.45	38	32	0.03	0.03
77	1629	1650	0.54	0.48	39	40	0.03	0.03
78	1650	1674	0.52	0.48	38	36	0.03	0.03
79	1674	1690	0.53	0.47	38	39	0.03	0.03
80	1690	1714	0.54	0.5	38	37	0.03	0.03
81	1714	1724	0.52	0.49	39	33	0.03	0.03
82	1724	1740	0.53	0.5	38	33	0.03	0.03
83	1740	1754	0.52	0.43	38	39	0.03	0.03
84	1754	1778	0.54	0.43	38	37	0.03	0.03
85	1778	1802	0.51	0.48	38	39	0.03	0.03

86	1802	1826	0.51	0.49	38	37	0.03	0.03
87	1826	1836	0.52	0.48	38	35	0.03	0.03
88	1836	1851	0.51	0.48	38	33	0.03	0.03
89	1851	1871	0.51	0.49	39	40	0.03	0.03
90	1871	1891	0.52	0.48	38	38	0.03	0.03
91	1891	1908	0.53	0.47	39	38	0.03	0.03
92	1908	1922	0.54	0.5	38	38	0.03	0.03
93	1922	1950	0.52	0.49	38	39	0.03	0.03
94	1950	1974	0.53	0.5	39	36	0.03	0.03
95	1974	1998	0.51	0.49	38	39	0.03	0.03
96	1998	2022	0.51	0.48	37	39	0.03	0.03
97	2022	2047	0.51	0.49	38	39	0.03	0.03
98	2047	2061	0.52	0.48	39	37	0.03	0.03
99	2061	2075	0.53	0.47	38	38	0.03	0.03
100	2075	2090	0.54	0.5	37	38	0.03	0.03
101	2090	2114	0.52	0.49	39	40	0.03	0.03
102	2114	2134	0.53	0.5	41	38	0.03	0.03
103	2134	2150	0.52	0.43	38	38	0.03	0.03
104	2150	2174	0.54	0.43	39	36	0.03	0.03
105	2174	2190	0.51	0.48	38	38	0.03	0.03
106	2190	2214	0.52	0.43	38	36	0.03	0.03
107	2214	2230	0.51	0.49	39	38	0.03	0.03
108	2230	2254	0.51	0.48	38	37	0.03	0.03

109	2254	2270	0.51	0.49	39	36	0.03	0.03
110	2270	2294	0.52	0.48	38	34	0.03	0.03
111	2294	2310	0.53	0.47	38	36	0.03	0.03
112	2310	2334	0.51	0.49	38	35	0.03	0.03
113	2334	2358	0.53	0.44	39	33	0.03	0.03
114	2358	2382	0.51	0.45	38	39	0.03	0.03
115	2382	2406	0.5	0.46	38	37	0.03	0.03
116	2406	2430	0.53	0.44	39	37	0.03	0.03
117	2430	2454	0.52	0.43	37	35	0.03	0.03
118	2454	2478	0.54	0.43	38	37	0.03	0.03
119	2478	2502	0.54	0.5	39	38	0.03	0.03
120	2502	2526	0.52	0.49	38	36	0.03	0.03
121	2526	2550	0.53	0.5	39	38	0.03	0.03
122	2550	2574	0.51	0.49	38	38	0.03	0.03
123	2574	2599	0.51	0.48	38	35	0.03	0.03
124	2599	2623	0.51	0.49	39	40	0.03	0.03
125	2623	2647	0.52	0.48	38	38	0.03	0.03
126	2647	2671	0.53	0.47	39	37	0.03	0.03
127	2671	2695	0.51	0.49	38	33	0.03	0.03
128	2695	2720	0.53	0.44	39	39	0.03	0.03
129	2720	2744	0.51	0.45	38	39	0.03	0.03
130	2744	2768	0.5	0.46	39	37	0.03	0.03
131	2768	2793	0.51	0.45	38	36	0.03	0.03

132	2793	2817	0.54	0.48	38	40	0.03	0.03
133	2817	2841	0.52	0.48	39	39	0.03	0.03
134	2841	2865	0.53	0.47	37	37	0.03	0.03
135	2865	2889	0.53	0.44	38	35	0.03	0.03
136	2889	2913	0.52	0.43	37	40	0.03	0.03
137	2913	2937	0.54	0.43	39	39	0.03	0.03
138	2937	2961	0.51	0.48	38	37	0.03	0.03
139	2961	2984	0.51	0.49	39	38	0.03	0.03
140	2984	3008	0.52	0.48	38	35	0.03	0.03
141	3008	3024	0.54	0.48	38	37	0.03	0.03

References

1. M. G. Kibria, R. Qiao, W. Yang, I. Boukahil, X. Kong, F. A. Chowdhury, M. L. Trudeau, W. Ji, H. Guo, F. J. Himpsel, L. Vayssieres and Z. Mi, *Adv. Mater.*, 2016, **28**, 8388-8397.
2. S. Vanka, E. Arca, S. Cheng, K. Sun, G. A. Botton, G. Teeter and Z. Mi, *Nano Lett.*, 2018, **18**, 6530-6537.
3. B. Zhou, X. Kong, S. Vanka, S. Chu, P. Ghamari, Y. Wang, N. Pant, I. Shih, H. Guo and Z. Mi, *Nat. Commun.*, 2018, **9**.
4. B. Zhou, X. Kong, S. Vanka, S. Cheng, N. Pant, S. Chu, P. Ghamari, Y. Wang, G. Botton, H. Cuo and Z. Mi, *Energ. Environ. Sci.*, 2019, DOI: 10.1039/c9ee01339c.
5. Z. Chen, T. F. Jaramillo, T. G. Deutsch, A. Kleiman-Shwarsctein, A. J. Forman, N. Gaillard, R. Garland, K. Takanabe, C. Heske, M. Sunkara, E. W. McFarland, K. Domen, E. L. Miller, J. A. Turner and H. N. Dinh, *J. Mater. Res.*, 2011, **25**, 3-16.
6. B. AlOtaibi, H. P. Nguyen, S. Zhao, M. G. Kibria, S. Fan and Z. Mi, *Nano Lett.*, 2013, **13**, 4356-4361.
7. L. A. King, T. R. Hellstern, J. Park, R. Sinclair and T. F. Jaramillo, *ACS Appl. Mater. Interfaces*, 2017, **9**, 36792-36798.
8. Y. Kuang, Q. Jia, G. Ma, T. Hisatomi, T. Minegishi, H. Nishiyama, M. Nakabayashi, N. Shibata, T. Yamada, A. Kudo and K. Domen, *Nat. Energ.*, 2016, **2**, 16191.
9. M. R. Shaner, S. Hu, K. Sun and N. S. Lewis, *Energ. Environ. Sci.*, 2015, **8**, 203-207.
10. W. Vijselaar, R. M. Tiggelaar, H. Gardeniers and J. Huskens, *ACS Energ. Lett.*, 2018, **3**, 1086-1092.
11. C. Ros, T. Andreu, M. D. Hernandez-Alonso, G. Penelas-Perez, J. Arbiol and J. R. Morante, *ACS Appl. Mater. Interfaces*, 2017, DOI: 10.1021/acsami.7b02996.

12. P. Dias, A. Vilanova, T. Lopes, L. Andrade and A. Mendes, *Nano Energ.*, 2016, **23**, 70-79.
13. B. Seger, D. S. Tilley, T. Pedersen, P. C. K. Vesborg, O. Hansen, M. Grätzel and I. Chorkendorff, *RSC Adv.*, 2013, **3**, 25902.
14. D. Bae, B. Seger, O. Hansen, P. C. K. Vesborg and I. Chorkendorff, *Chemelectrochem*, 2019, **6**, 106-109.
15. K. Sun, M. T. McDowell, A. C. Nielander, S. Hu, M. R. Shaner, F. Yang, B. S. Brunschwig and N. S. Lewis, *J. Phys. Chem. Lett.*, 2015, **6**, 592-598.
16. L. Zhang, T. Minegishi, M. Nakabayashi, Y. Suzuki, K. Seki, N. Shibata, J. Kubota and K. Domen, *Chem. Sci.*, 2015, **6**, 894-901.
17. Y. Nakato, Y. Iwakabe, M. Hiramoto and H. Tsubomura, *J. Electrochem. Soc.*, 1986, **133**, 900-904.